Robust entanglement of a micromechanical resonator with output optical fields

C. Genes, A. Mari, P. Tombesi, and D. Vitali
Dipartimento di Fisica, Università di Camerino, I-62032 Camerino (MC), Italy
(Received 11 June 2008; published 12 September 2008)

We perform an analysis of the optomechanical entanglement between the experimentally detectable output field of an optical cavity and a vibrating cavity end-mirror. We show that by a proper choice of the readout (mainly by a proper choice of detection bandwidth) one cannot only detect the already predicted intracavity entanglement but also optimize and increase it. This entanglement is explained as being generated by a scattering process owing to which strong quantum correlations between the mirror and the optical Stokes sideband are created. All-optical entanglement between scattered sidebands is also predicted, and it is shown that the mechanical resonator and the two sideband modes form a fully tripartite-entangled system capable of providing practicable and robust solutions for continuous-variable quantum-communication protocols.

DOI: 10.1103/PhysRevA.78.032316 PACS number(s): 03.67.Mn, 85.85.+j, 42.50.Wk, 42.50.Lc

I. INTRODUCTION

Mechanical resonators at the micro- and nanometer scale are now widely employed in the high-sensitivity detection of mass and forces [1–3]. The recent improvements in nanofabrication techniques suggest that in the near future these devices will reach the regime in which their sensitivity will be limited by the ultimate quantum limits set by the Heisenberg principle, as first suggested in the context of the detection of gravitational waves by the pioneering work of Braginsky and co-workers [4].

The experimental demonstration of genuine quantum states of macroscopic mechanical resonators with a mass in the nanogram-milligram range will represent an important step not only for the high-sensitivity detection of displacements and forces, but also for the foundations of physics. It would represent, in fact, a remarkable signature of the quantum behavior of a macroscopic object, allowing further light to be shed on the quantum-classical boundary [5]. Significant experimental [6–21] and theoretical [22–31] efforts are currently devoted to cooling such microresonators to their quantum ground state.

However, the generation of other examples of quantum states of a micromechanical resonator has been also considered recently. The most relevant examples are given by squeezed and entangled states. Squeezed states of nanomechanical resonators [32] are potentially useful for surpassing the standard quantum limit for position and force detection [4], and could be generated in different ways, using either coupling with a qubit [33] or measurement and feedback schemes [25,34]. Entanglement is instead the characteristic element of quantum theory, because it is responsible for correlations between observables that cannot be understood on the basis of local realistic theories [35]. For this reason, there has been an increasing interest in establishing the conditions under which entanglement between macroscopic objects can arise. Relevant experimental demonstrations in this direction are given by the entanglement between collective spins of atomic ensembles [36], and between Josephson-junction qubits [37]. Then, starting from the proposal of Ref. [38] in which two mirrors of a ring cavity are entangled by the radiation pressure of the cavity mode, many proposals involved nano- and micromechanical resonators eventually entangled with other systems. One can entangle a nanomechanical oscillator with a Cooper-pair box [39], while Ref. [40] studied how to entangle an array of nanomechanical oscillators. Further proposals suggested entangling two charge qubits [41] or two Josephson junctions [42] via nanomechanical resonators, or entangling two nanomechanical resonators via trapped ions [43], Cooper-pair boxes [44], or dc superconducting quantum interference devices (SQUIDS) [45]. More recently, schemes for entangling a superconducting coplanar waveguide field with a nanomechanical resonator, either via a Cooper-pair box within the waveguide [46], or via direct capacitive coupling [47], have been proposed.

After Ref. [38], other optomechanical systems have been proposed for entangling optical and/or mechanical modes by means of the radiation-pressure interaction. Reference [48] considered two mirrors of two different cavities illuminated with entangled light beams, while Refs. [49–52] considered different examples of double-cavity systems in which entanglement either between different mechanical modes or between a cavity mode and a vibrational mode of a cavity mirror was studied. References [53,54] considered the simplest scheme capable of generating stationary optomechanical entanglement, i.e., a single Fabry-Pérot cavity with either one [53] or two [54] movable mirrors.

Here we shall reconsider the Fabry-Pérot model of Ref. [53], which is remarkable for its simplicity and robustness against temperature of the resulting entanglement, and extend its study in various directions. In fact, entangled optomechanical systems could be profitably used for the realization of quantum-communication networks, in which the mechanical modes play the role of local nodes where quantum information can be stored and retrieved, and optical modes carry this information between the nodes. References [55–57] proposed a scheme of this kind, based on free-space light modes scattered by a single reflecting mirror, which could allow the implementation of continuous-variable (CV) quantum teleportation [55], quantum telecloning [56], and entanglement swapping [57]. Therefore, any quantum-communication application involves *traveling output* modes rather than intracavity ones, and it is important to study how the optomechanical entanglement generated within the cavity

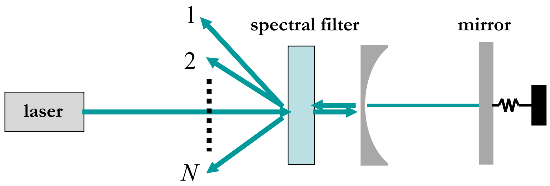

FIG. 1. (Color online) Scheme of the cavity, which is driven by a laser and has a vibrating mirror. With appropriate filters one can select N independent modes from the cavity output field.

is transferred to the output field. Furthermore, by considering the output field, one can adopt a multiplexing approach because, by means of spectral filters, one can always select many different traveling output modes originating from a single intracavity mode (see Fig. 1). One can therefore manipulate a multipartite system, eventually possessing multipartite entanglement. We shall develop a general theory showing how the entanglement between the mechanical resonator and optical output modes can be properly defined and calculated.

We shall see that, together with its output field, the single Fabry-Pérot cavity system of Ref. [53] represents the "cavity version" of the free-space scheme of Refs. [55,56]. In fact, as happens in this latter scheme, all the relevant dynamics induced by radiation-pressure interaction is carried by the two output modes corresponding to the first Stokes and anti-Stokes sidebands of the driving laser. In particular, the optomechanical entanglement with the intracavity mode is optimally transferred to the output Stokes sideband mode, which is, however, robustly entangled also with the anti-Stokes output mode. We shall see that the present Fabry-Pérot cavity system is preferable with respect to the free-space model of Refs. [55,56], because entanglement is achievable in a much more accessible experimental parameter region.

The outline of the paper is as follows. Section II gives a general description of the dynamics by means of the quantum Langevin equations (QLEs), Sec. III analyzes in detail the entanglement between the mechanical mode and the intracavity mode, while in Sec. IV we describe a general theory as to how a number of independent optical modes can be selected and defined, and their entanglement properties calculated. Section V is for concluding remarks.

II. SYSTEM DYNAMICS

We consider a driven optical cavity coupled by radiation pressure to a micromechanical oscillator. The typical experimental configuration is a Fabry-Pérot cavity with one mirror much lighter than the other (see, e.g., [8,10–13,20]), but our treatment applies to other configurations such as the silica toroidal microcavity of Refs. [14,19,58]. Radiation pressure couples each cavity mode with many vibrational normal modes of the movable mirror. However, by choosing the detection bandwidth so that only an isolated mechanical resonance significantly contributes to the detected signal, one can restrict consideration to a single mechanical oscillator, since intermode coupling due to mechanical nonlinearities are typically negligible (see also [59] for a more general treatment). The Hamiltonian of the system reads [60]

$$H = \hbar\omega_c a^\dagger a + \frac{1}{2}\hbar\omega_m(p^2+q^2) - \hbar G_0 a^\dagger a q + i\hbar E(a^\dagger e^{-i\omega_0 t} - a e^{i\omega_0 t}). \tag{1}$$

The first term describes the energy of the cavity mode, with lowering operator a ($[a,a^\dagger]=1$), cavity frequency ω_c, and decay rate κ. The second term gives the energy of the mechanical mode, modeled as a harmonic oscillator at frequency ω_m and described by dimensionless position and momentum operators q and p ($[q,p]=i$). The third term is the radiation-pressure coupling of rate $G_0=(\omega_c/L)\sqrt{\hbar/m\omega_m}$, where m is the effective mass of the mechanical mode [61], and L is an effective length that depends upon the cavity geometry: it coincides with the cavity length in the Fabry-Pérot case, and with the toroid radius in the case of Refs. [14,58]. The last term describes the input driving by a laser with frequency ω_0, where E is related to the input laser power P by $|E|=\sqrt{2P\kappa/\hbar\omega_0}$. One can adopt the single-cavity-mode description of Eq. (1) as long as one drives only one cavity mode and the mechanical frequency ω_m is much smaller than the cavity free spectral range $\mathcal{R}\sim c/L$. In this case, scattering of photons from the driven mode into other cavity modes is negligible [62].

The dynamics is also determined by the fluctuation-dissipation processes affecting both the optical and the mechanical modes. They can be taken into account in a fully consistent way [60] by considering the following set of nonlinear QLEs, written in the interaction picture with respect to $\hbar\omega_0 a^\dagger a$:

$$\dot{q} = \omega_m p, \tag{2a}$$

$$\dot{p} = -\omega_m q - \gamma_m p + G_0 a^\dagger a + \xi, \tag{2b}$$

$$\dot{a} = -(\kappa + i\Delta_0)a + iG_0 a q + E + \sqrt{2\kappa}a^{\rm in}, \tag{2c}$$

where $\Delta_0=\omega_c-\omega_0$. The mechanical mode is affected by a viscous force with damping rate γ_m and by a Brownian stochastic force with zero mean value ξ that obeys the correlation function [60,63,64]

$$\langle\xi(t)\xi(t')\rangle = \frac{\gamma_m}{\omega_m}\int\frac{d\omega}{2\pi}e^{-i\omega(t-t')}\omega\left[\coth\left(\frac{\hbar\omega}{2k_BT}\right)+1\right], \tag{3}$$

where k_B is the Boltzmann constant and T is the temperature of the reservoir of the micromechanical oscillator. The Brownian noise $\xi(t)$ is a Gaussian quantum stochastic process and its non-Markovian nature (neither its correlation function nor its commutator is proportional to a Dirac δ) guarantees that the QLEs of Eqs. (2) preserve the correct commutation relations between operators during the time evolution [60]. The cavity mode amplitude instead decays at the rate κ and is affected by the vacuum radiation input noise $a^{\rm in}(t)$, whose correlation functions are given by

$$\langle a^{\rm in}(t)a^{{\rm in},\dagger}(t')\rangle = [N(\omega_c)+1]\delta(t-t') \tag{4}$$

and

$$\langle a^{\mathrm{in},\dagger}(t)a^{\mathrm{in}}(t')\rangle = N(\omega_c)\delta(t-t'), \tag{5}$$

where $N(\omega_c)=[\exp(\hbar\omega_c/k_BT)-1]^{-1}$ is the equilibrium mean thermal photon number. At optical frequencies $\hbar\omega_c/k_BT \gg 1$ and therefore $N(\omega_c)\simeq 0$, so that only the correlation function of Eq. (4) is relevant. We shall neglect here technical noise sources, such as the amplitude and phase fluctuations of the driving laser. They can hinder the achievement of genuine quantum effects (see, e.g., [19,65]), but they could be easily accounted for by introducing fluctuations of the modulus and of the phase of the driving parameter E of Eq. (1) [65,66].

A. Linearization around the classical steady state and stability analysis

As shown in [53], significant optomechanical entanglement is achieved when radiation-pressure coupling is strong, which is realized when the intracavity field is very intense, i.e., for high-finesse cavities and enough driving power. In this limit (and if the system is stable), the system is characterized by a semiclassical steady state with the cavity mode in a coherent state with amplitude $\alpha_s=E/(\kappa+i\Delta)$, and the micromechanical mirror displaced by $q_s=G_0|\alpha_s|^2/\omega_m$ (see Refs. [30,53,67] for details). The expression giving the intracavity amplitude α_s is actually an implicit nonlinear equation for α_s because

$$\Delta = \Delta_0 - \frac{G_0^2|\alpha_s|^2}{\omega_m} \tag{6}$$

is the effective cavity detuning including the effect of the stationary radiation pressure. As shown in Refs. [30,53], when $|\alpha_s|\gg 1$ the quantum dynamics of the fluctuations around the steady state is well described by linearizing the nonlinear QLEs of Eqs. (2). Defining the cavity field fluctuation quadratures $\delta X \equiv (\delta a+\delta a^\dagger)/\sqrt{2}$ and $\delta Y \equiv (\delta a-\delta a^\dagger)/i\sqrt{2}$, and the corresponding Hermitian input noise operators $X^{\mathrm{in}} \equiv (a^{\mathrm{in}}+a^{\mathrm{in},\dagger})/\sqrt{2}$ and $Y^{\mathrm{in}} \equiv (a^{\mathrm{in}}-a^{\mathrm{in},\dagger})/i\sqrt{2}$, the linearized QLEs can be written in the following compact matrix form [53]:

$$\dot{u}(t) = Au(t) + n(t), \tag{7}$$

where $u^T(t)=(\delta q(t),\delta p(t),\delta X(t),\delta Y(t))^T$ (the superscript T denotes the transposition) is the vector of CV fluctuation operators, $n^T(t)=(0,\xi(t),\sqrt{2\kappa}X^{\mathrm{in}}(t),\sqrt{2\kappa}Y^{\mathrm{in}}(t))^T$ the corresponding vector of noises, and A the matrix

$$A = \begin{pmatrix} 0 & \omega_m & 0 & 0 \\ -\omega_m & -\gamma_m & G & 0 \\ 0 & 0 & -\kappa & \Delta \\ G & 0 & -\Delta & -\kappa \end{pmatrix}, \tag{8}$$

where

$$G = G_0\alpha_s\sqrt{2} = \frac{2\omega_c}{L}\sqrt{\frac{P\kappa}{m\omega_m\omega_0(\kappa^2+\Delta^2)}} \tag{9}$$

is the *effective* optomechanical coupling (we have chosen the phase reference so that α_s is real and positive). When $\alpha_s \gg 1$, one has $G \gg G_0$, and therefore the generation of significant optomechanical entanglement is facilitated in this linearized regime.

The formal solution of Eq. (7) is $u(t)=M(t)u(0)+\int_0^t ds\, M(s)n(t-s)$, where $M(t)=\exp(At)$. The system is stable and reaches its steady state for $t\to\infty$ when all the eigenvalues of A have negative real parts so that $M(\infty)=0$. The stability conditions can be derived by applying the Routh-Hurwitz criterion [68], yielding the following two nontrivial conditions on the system parameters:

$$s_1 = 2\gamma_m\kappa\{[\kappa^2+(\omega_m-\Delta)^2][\kappa^2+(\omega_m+\Delta)^2]+\gamma_m[(\gamma_m+2\kappa)\times(\kappa^2+\Delta^2)+2\kappa\omega_m^2]\}+\Delta\omega_m G^2(\gamma_m+2\kappa)^2 > 0, \tag{10a}$$

$$s_2 = \omega_m(\kappa^2+\Delta^2) - G^2\Delta > 0, \tag{10b}$$

which will be considered to be satisfied from now on. Notice that when $\Delta>0$ (the laser is red detuned with respect to the cavity) the first condition is always satisfied and only s_2 is relevant, while when $\Delta<0$ (blue-detuned laser) the second condition is always satisfied and only s_1 matters.

When the system is stable, the eigenvalues of A also determine the relaxation time, i.e., the time required for the system to reach the steady state. In fact, this time is determined by the eigenvalue of A whose real part is closest to zero: the relaxation time is equal to the inverse of the absolute value of this real part. As expected, in the absence of radiation-pressure coupling, $G=0$, the relaxation time is given by $\min\{\gamma_m^{-1},\kappa^{-1}\}$ and therefore by the mechanical relaxation time γ_m^{-1}, because it is typically $\kappa \gg \gamma_m$. For generic parameter values and optomechanical couplings the relaxation time has an involved expression and depends upon all the parameters; however, it becomes larger and larger if the instability threshold is approached and it becomes infinite exactly at threshold.

B. Correlation matrix of the quantum fluctuations of the system

The steady state of the bipartite quantum system formed by the vibrational mode of interest and the fluctuations of the intracavity mode can be fully characterized. In fact, the quantum noises ξ and a^{in} are zero-mean quantum Gaussian noises and the dynamics is linearized, and, as a consequence, the steady state of the system is a zero-mean bipartite Gaussian state, fully characterized by its 4×4 correlation matrix (CM) $V_{ij}=[\langle u_i(\infty)u_j(\infty)+u_j(\infty)u_i(\infty)\rangle]/2$. Starting from Eq. (7), this steady-state CM can be determined in two equivalent ways. Using the Fourier transforms $\tilde{u}_i(\omega)$ of $u_i(t)$, one has

$$V_{ij}(t) = \int\int \frac{d\omega\, d\omega'}{4\pi} e^{-it(\omega+\omega')}\langle \tilde{u}_i(\omega)\tilde{u}_j(\omega') + \tilde{u}_j(\omega')\tilde{u}_i(\omega)\rangle. \tag{11}$$

Then, by Fourier transforming Eq. (7) and the correlation functions of the noises, Eqs. (3) and (4), one gets

$$\frac{\langle \tilde{u}_i(\omega)\tilde{u}_j(\omega') + \tilde{u}_j(\omega')\tilde{u}_i(\omega)\rangle}{2} = [\tilde{M}(\omega)D(\omega)\tilde{M}(\omega')^T]_{ij}\delta(\omega+\omega'), \tag{12}$$

where we have defined the 4×4 matrices

$$\tilde{M}(\omega) = (i\omega + A)^{-1} \tag{13}$$

and

$$D(\omega) = \begin{pmatrix} 0 & 0 & 0 & 0 \\ 0 & \frac{\gamma_m \omega}{\omega_m}\coth\left(\frac{\hbar\omega}{2k_BT}\right) & 0 & 0 \\ 0 & 0 & \kappa & 0 \\ 0 & 0 & 0 & \kappa \end{pmatrix}. \tag{14}$$

The $\delta(\omega+\omega')$ factor is a consequence of the stationarity of the noises, which implies the stationarity of the CM V: in fact, inserting Eq. (12) into Eq. (11), one gets that V is time independent and can be written as

$$V = \int d\omega\, \tilde{M}(\omega)D(\omega)\tilde{M}(\omega)^{\dagger}. \tag{15}$$

It is, however, reasonable to simplify this exact expression for the steady-state CM, by appropriately approximating the thermal noise contribution $D_{22}(\omega)$ in Eq. (14). In fact $k_BT/\hbar \simeq 10^{11}$ s^{-1} even at cryogenic temperatures, and it is therefore much larger than all the other typical frequency scales, which are at most of the order of 10^9 Hz. The integrand in Eq. (15) goes rapidly to zero at $\omega \sim 10^{11}$ Hz, and therefore one can safely neglect the frequency dependence of $D_{22}(\omega)$ by approximating it with its zero-frequency value

$$\frac{\gamma_m\omega}{\omega_m}\coth\left(\frac{\hbar\omega}{2k_BT}\right) \simeq \gamma_m\frac{2k_BT}{\hbar\omega_m} \simeq \gamma_m(2\bar{n}+1), \tag{16}$$

where $\bar{n}=[\exp(\hbar\omega_m/k_BT)-1]^{-1}$ is the mean thermal excitation number of the resonator.

It is easy to verify that assuming a frequency-independent diffusion matrix D is equivalent to making the following Markovian approximation to the quantum Brownian noise $\xi(t)$:

$$\langle \xi(t)\xi(t') + \xi(t')\xi(t)\rangle/2 \simeq \gamma_m(2n+1)\delta(t-t'), \tag{17}$$

which is known to be valid also in the limit of a very high mechanical quality factor $\mathcal{Q}=\omega_m/\gamma_m \to \infty$ [69]. Within this Markovian approximation, the above frequency domain treatment is equivalent to the time domain derivation considered in [53] which, starting from the formal solution of Eq. (7), arrives at

$$V_{ij}(\infty) = \sum_{k,l}\int_0^{\infty} ds \int_0^{\infty} ds' M_{ik}(s)M_{jl}(s')D_{kl}(s-s'), \tag{18}$$

where $D_{kl}(s-s')=[\langle n_k(s)n_l(s')+n_l(s')n_k(s)\rangle]/2$ is the matrix of the stationary noise correlation functions. The Markovian approximation of the thermal noise on the mechanical resonator yields $D_{kl}(s-s')=D_{kl}\delta(s-s')$, with $D=\mathrm{Diag}[0,\gamma_m(2\bar{n}+1),\kappa,\kappa]$, so that Eq. (18) becomes

$$V = \int_0^{\infty} ds\, M(s)DM(s)^T, \tag{19}$$

which is equivalent to Eq. (15) whenever D does not depend upon ω. When the stability conditions are satisfied $[M(\infty)=0]$, Eq. (19) is equivalent to the following Lyapunov equation for the steady-state CM:

$$AV + VA^T = -D, \tag{20}$$

which is a linear equation for V and can be straightforwardly solved; but the general exact expression is too cumbersome and will not be reported here.

III. OPTOMECHANICAL ENTANGLEMENT WITH THE INTRACAVITY MODE

In order to establish the conditions under which the optical mode and the mirror vibrational mode are entangled, we consider the logarithmic negativity $E_{\mathcal{N}}$, which can be defined as [70]

$$E_{\mathcal{N}} = \max(0, -\ln 2\eta^-), \tag{21}$$

where $\eta^- \equiv 2^{-1/2}\{\Sigma(V)-[\Sigma(V)^2-4\det V]^{1/2}\}^{1/2}$, with $\Sigma(V) \equiv \det V_m + \det V_c - 2\det V_{mc}$, and we have used the 2×2 block form of the CM,

$$V \equiv \begin{pmatrix} V_m & V_{mc} \\ V_{mc}^T & V_c \end{pmatrix}. \tag{22}$$

Therefore, a Gaussian state is entangled if and only if $\eta^- < 1/2$, which is equivalent to Simon's necessary and sufficient entanglement nonpositive partial transpose criterion for Gaussian states [71], which can be written as $4\det V < \Sigma - 1/4$.

A. Correspondence with the down-conversion process

As already shown in [28–30], many features of the radiation-pressure interaction in the cavity can be understood by considering that the driving laser light is scattered by the vibrating cavity boundary mostly at the first Stokes $(\omega_0 - \omega_m)$ and anti-Stokes $(\omega_0+\omega_m)$ sidebands. Therefore we expect that the optomechanical interaction and eventually entanglement will be enhanced when the cavity is resonant with one of the two sidebands, i.e., when $\Delta = \pm\omega_m$.

It is useful to introduce the mechanical annihilation operator $\delta b = (\delta q + i\delta p)/\sqrt{2}$, obeying the following QLE:

$$\dot{\delta b} = -i\omega_m\delta b - \frac{\gamma_m}{2}(\delta b - \delta b^{\dagger}) + i\frac{G}{2}(\delta a^{\dagger} + \delta a) + \frac{\xi}{\sqrt{2}}. \tag{23}$$

Moving to another interaction picture by introducing the slowly moving operators with tildes, $\delta b(t) = \delta\tilde{b}(t)e^{-i\omega_m t}$ and $\delta a(t) = \delta\tilde{a}(t)e^{-i\Delta t}$, we obtain from the linearized version of Eqs. (2c) and (23) the following QLEs:

$$\delta\dot{\tilde{b}} = -\frac{\gamma_m}{2}(\delta\tilde{b} - \delta\tilde{b}^\dagger e^{2i\omega_m t}) + \sqrt{\gamma_m} b^{\text{in}} + i\frac{G}{2}(\delta\tilde{a}^\dagger e^{i(\Delta+\omega_m)t} + \delta\tilde{a} e^{i(\omega_m-\Delta)t}), \tag{24}$$

$$\delta\dot{\tilde{a}} = -\kappa\delta\tilde{a} + i\frac{G}{2}(\delta\tilde{b}^\dagger e^{i(\Delta+\omega_m)t} + \delta\tilde{b} e^{i(\Delta-\omega_m)t}) + \sqrt{2\kappa}\tilde{a}^{\text{in}}. \tag{25}$$

Note that we have introduced two noise operators: (i) $\tilde{a}^{\text{in}}(t) = a^{\text{in}}(t)e^{i\Delta t}$, possessing the same correlation function as $a^{\text{in}}(t)$; (ii) $b^{\text{in}}(t) = \xi(t)e^{i\omega_m t}/\sqrt{2}$ which, in the limit of large ω_m, acquires the correlation functions [72]

$$\langle b^{in,\dagger}(t) b^{\text{in}}(t')\rangle = \bar{n}\delta(t-t'), \tag{26}$$

$$\langle b^{\text{in}}(t) b^{in,\dagger}(t')\rangle = (\bar{n}+1)\delta(t-t'). \tag{27}$$

Equations (24) and (25), are still equivalent to the linearized QLEs of Eq. (7), but now we particularize them by choosing $\Delta = \pm\omega_m$. If the cavity is resonant with the Stokes sideband of the driving laser, $\Delta = -\omega_m$, one gets

$$\delta\dot{\tilde{b}} = -\frac{\gamma_m}{2}\delta\tilde{b} + \frac{\gamma_m}{2}\delta\tilde{b}^\dagger e^{2i\omega_m t} + i\frac{G}{2}\delta\tilde{a}^\dagger + i\frac{G}{2}\delta\tilde{a} e^{2i\omega_m t} + \sqrt{\gamma_m} b^{\text{in}}, \tag{28}$$

$$\delta\dot{\tilde{a}} = -\kappa\delta\tilde{a} + i\frac{G}{2}\delta\tilde{b}^\dagger + i\frac{G}{2}\delta\tilde{b} e^{2i\omega_m t} + \sqrt{2\kappa}\tilde{a}^{\text{in}}, \tag{29}$$

while when the cavity is resonant with the anti-Stokes sideband of the driving laser, $\Delta = \omega_m$, one gets

$$\delta\dot{\tilde{b}} = -\frac{\gamma_m}{2}\delta\tilde{b} + \frac{\gamma_m}{2}\delta\tilde{b}^\dagger e^{2i\omega_m t} + i\frac{G}{2}\delta\tilde{a} + i\frac{G}{2}\delta\tilde{a}^\dagger e^{-2i\omega_m t} + \sqrt{\gamma_m} b^{\text{in}}, \tag{30}$$

$$\delta\dot{\tilde{a}} = -\kappa\delta\tilde{a} + i\frac{G}{2}\delta\tilde{b} + i\frac{G}{2}\delta\tilde{b}^\dagger e^{-2i\omega_m t} + \sqrt{2\kappa}\tilde{a}^{\text{in}}. \tag{31}$$

From Eqs. (28) and (29) we see that, for a blue-detuned driving laser, $\Delta = -\omega_m$, the cavity mode and mechanical resonator are coupled via two kinds of interactions: (i) a down-conversion process characterized by $\delta\tilde{b}^\dagger\delta\tilde{a}^\dagger + \delta\tilde{a}\delta\tilde{b}$, which is resonant, and (ii) a beam-splitter-like process characterized by $\delta\tilde{b}^\dagger\delta\tilde{a} + \delta\tilde{a}^\dagger\delta\tilde{b}$, which is off resonant. Since the beam splitter interaction is not able to entangle modes starting from classical input states [73], and it is also off resonant in this case, one can invoke the rotating wave approximation (RWA) (which is justified in the limit of $\omega_m \gg G, \kappa$) and simplify the interaction to a down-conversion process, which is known to generate bipartite entanglement. In the red-detuned driving laser case, Eqs. (30) and (31) show that the two modes are strongly coupled by a beam-splitter-like interaction, while the down-conversion process is off resonant. If one chose to make the RWA in this case, one would be left with an effective beam splitter interaction which cannot entangle. Therefore, in the RWA limit $\omega_m \gg G, \kappa$, the best regime for strong optomechanical entanglement is when the laser is blue detuned from the cavity resonance and down-conversion is enhanced. However, as will be seen in the following section, this is hindered by instability and one is rather forced to work in the opposite regime of a red-detuned laser where instability occurs only at large values of G.

B. Entanglement in the blue-detuned regime

The CM of the Gaussian steady state of the bipartite system can be obtained from Eqs. (28)–(31), in the RWA limit, with the techniques of the previous section (see also [47])

$$V \equiv V^\pm = \begin{pmatrix} V_{11}^\pm & 0 & 0 & V_{14}^\pm \\ 0 & V_{11}^\pm & \pm V_{14}^\pm & 0 \\ 0 & \pm V_{14}^\pm & V_{33}^\pm & 0 \\ V_{14}^\pm & 0 & 0 & V_{33}^\pm \end{pmatrix}, \tag{32}$$

where the upper (lower) sign corresponds to the blue-(red-)detuned case, and

$$V_{11}^\pm = \bar{n} + \frac{1}{2} + \frac{2G^2\kappa[1/2 \pm (\bar{n}+1/2)]}{(\gamma_m + 2\kappa)(2\gamma_m\kappa \mp G^2)}, \tag{33a}$$

$$V_{33}^\pm = \frac{1}{2} + \frac{G^2\gamma_m(\bar{n}+1/2 \pm 1/2)}{(\gamma_m + 2\kappa)(2\gamma_m\kappa \mp G^2)}, \tag{33b}$$

$$V_{14}^\pm = \frac{2G\gamma_m\kappa(\bar{n}+1/2 \pm 1/2)}{(\gamma_m + 2\kappa)(2\gamma_m\kappa \mp G^2)}. \tag{33c}$$

For clarity we have included the red-detuned case in the RWA and we see that $\det V_{mc}^\pm = \mp(V_{14}^\pm)^2$, i.e., is non-negative in this latter case, which is a sufficient condition for the separability of bipartite states [71]. Of course, this is expected, since it is just the beam splitter interaction that generates this CM. Thus, in the weak optomechanical coupling regime of the RWA limit, entanglement is obtained only for a blue-detuned laser, $\Delta = -\omega_m$. However, the amount of achievable optomechanical entanglement at the steady state is seriously limited by the stability condition of Eq. (10a), which in the RWA limit $\Delta = -\omega_m \gg \kappa, \gamma_m$ simplifies to $G < \sqrt{2\kappa\gamma_m}$. Since one needs a small mechanical dissipation rate γ_m in order to see quantum effects, this means a very low maximum value for G. The logarithmic negativity $E_{\mathcal{N}}$ is an increasing function of the effective optomechanical coupling G (as expected), and therefore the stability condition puts a strong upper bound also on $E_{\mathcal{N}}$. In fact, it is possible to prove that the following bound on $E_{\mathcal{N}}$ exists:

$$E_{\mathcal{N}} \leq \ln\left(\frac{1 + G/\sqrt{2\kappa\gamma_m}}{1+\bar{n}}\right), \tag{34}$$

showing that $E_{\mathcal{N}} \leq \ln 2$ and above all that entanglement is extremely fragile with respect to temperature in the RWA limit, because, due to the stability condition, $E_{\mathcal{N}}$ vanishes as soon as $\bar{n} \geq 1$.

C. Entanglement in the red-detuned regime

We conclude that, due to instability, one can find significant optomechanical entanglement, which is also robust

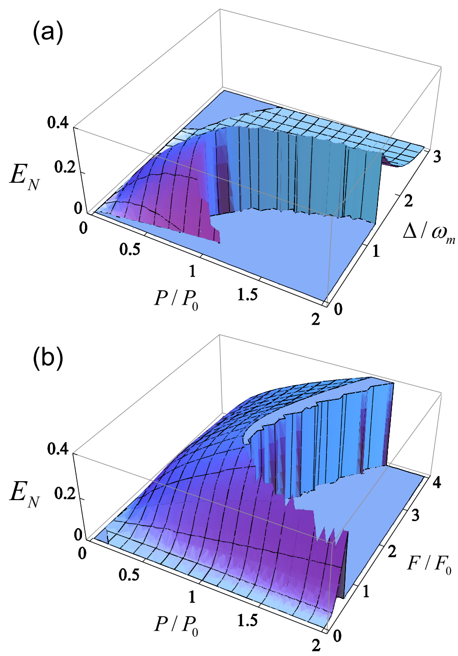

FIG. 2. (Color online) (a) Logarithmic negativity $E_{\mathcal{N}}$ versus the normalized detuning Δ/ω_m and normalized input power P/P_0, (P_0=50 mW) at a fixed value of the cavity finesse $F=F_0=1.67\times 10^4$; (b) $E_{\mathcal{N}}$ versus the normalized finesse F/F_0 and normalized input power P/P_0 at a fixed detuning $\Delta=\omega_m$. Parameter values are $\omega_m/2\pi=10$ MHz, $\mathcal{Q}=10^5$, mass $m=10$ ng, a cavity of length $L=1$ mm driven by a laser with wavelength 810 nm, yielding $G_0=0.95$ KHz and a cavity bandwidth $\kappa=0.9\omega_m$ when $F=F_0$. We have assumed a reservoir temperature for the mirror $T=0.4$ K, corresponding to $\bar{n}\simeq 833$. The sudden drop to zero of $E_{\mathcal{N}}$ corresponds to entering the instability region.

against temperature, only far from the RWA regime, in the strong coupling regime in the region with positive Δ, because Eq. (10b) allows for higher values of G. This is confirmed by Fig. 2, where $E_{\mathcal{N}}$ is plotted versus the normalized detuning Δ/ω_m and the normalized input power P/P_0 ($P_0=50$ mW) at a fixed value of the cavity finesse $F=F_0=1.67\times 10^4$ in Fig. 2(a), and versus the normalized finesse F/F_0 and normalized input power P/P_0 at a fixed cavity detuning $\Delta=\omega_m$ in Fig. 2(b). We have assumed an experimentally achievable situation, i.e., a mechanical mode with $\omega_m/2\pi=10$ MHz, $\mathcal{Q}=10^5$, mass $m=10$ ng, and a cavity of length $L=1$ mm, driven by a laser with wavelength 810 nm, yielding $G_0=0.95$ kHz and a cavity bandwidth $\kappa=0.9\omega_m$ when $F=F_0$. We have assumed a reservoir temperature for the mirror $T=0.4$K, corresponding to $\bar{n}\simeq 833$. Figure 2(a) shows that $E_{\mathcal{N}}$ is peaked around $\Delta\simeq\omega_m$, even though the peak shifts to larger values of Δ at larger input powers P. For increasing P at fixed Δ, $E_{\mathcal{N}}$ increases, even though at the same time the instability region (where the plot is suddenly interrupted) widens. In Fig. 2(b) we fixed the detuning at $\Delta=\omega_m$ (i.e., the cavity is resonant with the anti-Stokes sideband of the laser) and varied both the input power and the cavity finesse. We see again that $E_{\mathcal{N}}$ is maximum just at the instability threshold and also that, once the finesse has reached a sufficiently large value, $F\simeq F_0$, $E_{\mathcal{N}}$ roughly saturates at larger values of F. That is, one gets an optimal optomechanical entanglement when $\kappa\simeq\omega_m$ and moving into the well-resolved sideband limit $\kappa\ll\omega_m$ does not improve the value of $E_{\mathcal{N}}$. The parameter region analyzed is analogous to that considered in [53], where it has been shown that this optomechanical entanglement is extremely robust with respect to the temperature of the reservoir of the mirror, since it persists to more than 20 K.

D. Relationship between entanglement and cooling

As discussed in detail in [28–31], the same cavity–mechanical-resonator system can be used for realizing cavity-mediated optical cooling of the mechanical resonator via the back action of the cavity mode [23]. In particular, back action cooling is optimized just in the same regime where $\Delta\simeq\omega_m$. This fact is easily explained by taking into account the scattering of the laser light by the oscillating mirror into the Stokes and anti-Stokes sidebands. The generation of an anti-Stokes photon takes away a vibrational phonon and is responsible for cooling, while the generation of a Stokes photon heats the mirror by producing an extra phonon. If the cavity is resonant with the anti-Stokes sideband, cooling prevails and one has a positive net laser cooling rate given by the difference of the scattering rates.

It is therefore interesting to discuss the relation between optimal optomechanical entanglement and optimal cooling of the mechanical resonator. This can easily performed because the steady-state CM V determines also the resonator energy, since the effective stationary excitation number of the resonator is given by $n_{\rm eff}=(V_{11}+V_{22}-1)/2$ (see Ref. [30] for the exact expression of these matrix elements giving the steady-state position and momentum resonator variances). In Fig. 3 we have plotted $n_{\rm eff}$ under exactly the same parameter conditions as in Fig. 2. We see that ground state cooling is approached ($n_{\rm eff}<1$) simultaneously with a significant entanglement. This shows that a significant back action cooling of the resonator by the cavity mode is an important condition for achieving an entangled steady state that is robust against the effects of the resonator thermal bath.

Nonetheless, entanglement and cooling are different phenomena and optimizing one does not generally also optimize the other. This can be seen by comparing Figs. 2 and 3: $E_{\mathcal{N}}$ is maximized always just at the instability threshold, i.e., for the maximum possible optomechanical coupling, while this is not true for $n_{\rm eff}$, which is instead minimized quite far from the instability threshold. For a more clear understanding we make use of some of the results obtained for ground state cooling in Refs. [28–30]. In the perturbative limit where $G\ll\omega_m,\kappa$, one can define scattering rates into the Stokes (A_+) and anti-Stokes (A_-) sidebands as

$$A_{\pm}=\frac{G^2\kappa/2}{\kappa^2+(\Delta\pm\omega_m)^2}, \tag{35}$$

so that the net laser cooling rate is given by

$$\Gamma=A_- - A_+ > 0. \tag{36}$$

The final occupancy of the mirror mode is consequently given by [28–30]

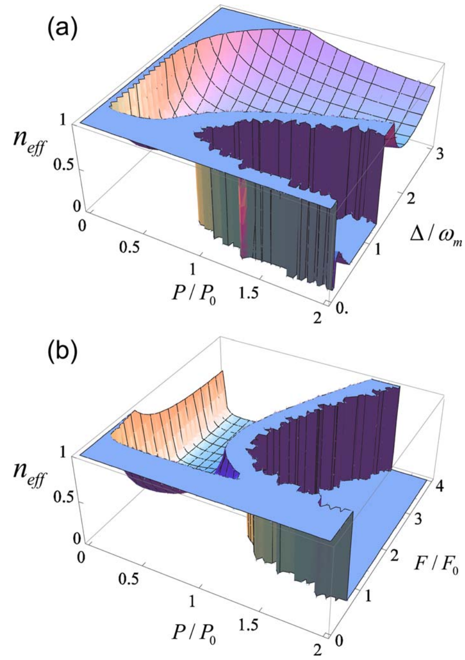

FIG. 3. (Color online) (a) Effective stationary excitation number of the resonator $n_{\rm eff}$ versus the normalized detuning Δ/ω_m and normalized input power P/P_0 (P_0=50 mW) at a fixed value of the cavity finesse $F=F_0=1.67\times10^4$; (b) $n_{\rm eff}$ versus the normalized finesse F/F_0 and normalized input power P/P_0 at a fixed detuning $\Delta=\omega_m$. Parameter values are the same as in Fig. 2. Again, the sudden drop to zero corresponds to entering the instability region.

$$n_{\rm eff}=\frac{\gamma_m\bar{n}}{\gamma_m+\Gamma}+\frac{A_+}{\gamma_m+\Gamma}, \tag{37}$$

where the first term in the right-hand side is the minimized thermal noise, which can be made vanishingly small provided that $\gamma_m \ll \Gamma$, while the second term shows residual heating produced by Stokes scattering off the vibrational ground state. When $\Gamma \gg \gamma_m\bar{n}$, the lower bound for $n_{\rm eff}$ is practically set by the ratio A_+/Γ. However, as soon as G is increased for improving the entanglement generation, scattering into higher-order sidebands takes place, with rates proportional to higher powers of G. As a consequence, even though the effective thermal noise is still close to zero, residual scattering off the ground state takes place at a rate that can be much higher than A_+. This can be seen more clearly in the exact expression of $\langle\delta q^2\rangle=V_{11}$ given in [30], which is shown to diverge at the threshold given by Eq. (10b).

The net laser cooling rate Γ determines also the relaxation time of the optomechanical system. In fact, $\gamma_m+\Gamma$ is the effective relaxation rate of the mechanical oscillator in the presence of the radiation-pressure interaction. Therefore the time required to reach the steady state is essentially given by the inverse of the smallest number between κ and $\gamma_m+\Gamma$.

IV. OPTOMECHANICAL ENTANGLEMENT WITH CAVITY OUTPUT MODES

The above analysis of the entanglement between the mechanical mode of interest and the intracavity mode provides a detailed description of the internal dynamics of the system, but it is not of direct use for practical applications. In fact, one typically does not have direct access to the intracavity field, but one detects and manipulates only the cavity output field. For example, for any quantum-communication application, it is much more important to analyze the entanglement of the mechanical mode with the *optical cavity output*, i.e., how the intracavity entanglement is transferred to the output field. Moreover, considering the output field provides further options. In fact, by means of spectral filters, one can always select many different traveling output modes originating from a single intracavity mode, and this gives the opportunity to easily produce and manipulate a multipartite system, eventually possessing multipartite entanglement.

A. General definition of cavity output modes

The intracavity field $\delta a(t)$ and its output are related by the usual input-output relation [63]

$$a^{\rm out}(t)=\sqrt{2\kappa}\,\delta a(t)-a^{\rm in}(t), \tag{38}$$

where the output field possesses the same correlation functions as the optical input field $a^{\rm in}(t)$ and the same commutation relation, i.e., the only nonzero commutator is $[a^{\rm out}(t),a^{\rm out}(t')^\dagger]=\delta(t-t')$. From the continuous output field $a^{\rm out}(t)$ one can extract many independent optical modes, by selecting different time intervals or, equivalently, different frequency intervals (see, e.g., [74]). One can define a generic set of N output modes by means of the corresponding annihilation operators

$$a_k^{\rm out}(t)=\int_{-\infty}^{t} ds\, g_k(t-s)a^{\rm out}(s), \quad k=1,\ldots,N, \tag{39}$$

where $g_k(s)$ is the causal filter function defining the kth output mode. These annihilation operators describe N independent optical modes when $[a_j^{\rm out}(t),a_k^{\rm out}(t)^\dagger]=\delta_{jk}$, which is satisfied when

$$\int_0^\infty ds\, g_j(s)^* g_k(s)=\delta_{jk}, \tag{40}$$

i.e., the N filter functions $g_k(t)$ form an orthonormal set of square-integrable functions in $[0,\infty)$. The situation can be equivalently described in the frequency domain: taking the Fourier transform of Eq. (39), one has

$$\tilde{a}_k^{\rm out}(\omega)=\int_{-\infty}^{\infty}\frac{dt}{\sqrt{2\pi}}a_k^{\rm out}(t)e^{i\omega t}=\sqrt{2\pi}\tilde{g}_k(\omega)a^{\rm out}(\omega), \tag{41}$$

where $\tilde{g}_k(\omega)$ is the Fourier transform of the filter function. An explicit example of an orthonormal set of filter functions is given by

$$g_k(t)=\frac{\theta(t)-\theta(t-\tau)}{\sqrt{\tau}}e^{-i\Omega_k t} \tag{42}$$

(θ denotes the Heaviside step function) provided that Ω_k and τ satisfy the condition

$$\Omega_j - \Omega_k = \frac{2\pi}{\tau}p, \quad \text{integer } p. \tag{43}$$

These functions describe a set of independent optical modes, each centered around the frequency Ω_k and with time duration τ, i.e., frequency bandwidth $\sim 1/\tau$, since

$$\tilde{g}_k(\omega) = \sqrt{\frac{\tau}{2\pi}} e^{i(\omega-\Omega_k)\tau/2} \frac{\sin[(\omega-\Omega_k)\tau/2]}{(\omega-\Omega_k)\tau/2}. \tag{44}$$

When the central frequencies differ by an integer multiple of $2\pi/\tau$, the corresponding modes are independent due to the destructive interference of the oscillating parts of the spectrum.

B. Stationary correlation matrix of output modes

The entanglement between the output modes defined above and the mechanical mode is fully determined by the corresponding $(2N+2)\times(2N+2)$ CM, which is defined by

$$V_{ij}^{\mathrm{out}}(t) = \frac{1}{2}\langle u_i^{\mathrm{out}}(t)u_j^{\mathrm{out}}(t) + u_j^{\mathrm{out}}(t)u_i^{\mathrm{out}}(t)\rangle, \tag{45}$$

where

$$u^{\mathrm{out}}(t) = (\delta q(t), \delta p(t), X_1^{\mathrm{out}}(t), Y_1^{\mathrm{out}}(t), \ldots, X_N^{\mathrm{out}}(t), Y_N^{\mathrm{out}}(t))^T \tag{46}$$

is the vector formed by the mechanical position and momentum fluctuations and by the amplitude, $X_k^{\mathrm{out}}(t)=[a_k^{\mathrm{out}}(t)+a_k^{\mathrm{out}}(t)^\dagger]/\sqrt{2}$, and phase, $Y_k^{\mathrm{out}}(t)=[a_k^{\mathrm{out}}(t)-a_k^{\mathrm{out}}(t)^\dagger]/i\sqrt{2}$, quadratures of the N output modes. The vector $u^{\mathrm{out}}(t)$ properly describes $N+1$ independent CV bosonic modes, and in particular the mechanical resonator is independent of (i.e., it commutes with) the N optical output modes because the latter depend upon the output field at previous times only ($s<t$). From the definition of $u^{\mathrm{out}}(t)$, of the output modes of Eq. (39), and the input-output relation of Eq. (38), one can write

$$u_i^{\mathrm{out}}(t) = \int_{-\infty}^{t} ds\, T_{ik}(t-s)u_k^{\mathrm{ext}}(s) - \int_{-\infty}^{t} ds\, T_{ik}(t-s)n_k^{\mathrm{ext}}(s), \tag{47}$$

where

$$u^{\mathrm{ext}}(t) = (\delta q(t), \delta p(t), X(t), Y(t), \ldots, X(t), Y(t))^T \tag{48}$$

is the $(2N+2)$-dimensional vector obtained by extending the four-dimensional vector $u(t)$ of the preceding section by repeating N times the components related to the optical cavity mode, and

$$n^{\mathrm{ext}}(t) = \frac{1}{\sqrt{2\kappa}}(0,0,X_{\mathrm{in}}(t), Y_{\mathrm{in}}(t), \ldots, X_{\mathrm{in}}(t), Y_{\mathrm{in}}(t))^T \tag{49}$$

is the analogous extension of the noise vector $n(t)$ of the former section without, however, the noise acting on the mechanical mode. In Eq. (47) we have also introduced the $(2N+2)\times(2N+2)$ block matrix consisting of $N+1$ two-dimensional blocks,

$$T(t) = \begin{pmatrix} \delta(t) & 0 & 0 & 0 & 0 & 0 & \ldots \\ 0 & \delta(t) & 0 & 0 & 0 & 0 & \ldots \\ 0 & 0 & \sqrt{2\kappa}\,\mathrm{Re}\, g_1(t) & -\sqrt{2\kappa}\,\mathrm{Im}\, g_1(t) & 0 & 0 & \ldots \\ 0 & 0 & \sqrt{2\kappa}\,\mathrm{Im}\, g_1(t) & \sqrt{2\kappa}\,\mathrm{Re}\, g_1(t) & 0 & 0 & \ldots \\ 0 & 0 & 0 & 0 & \sqrt{2\kappa}\,\mathrm{Re}\, g_2(t) & -\sqrt{2\kappa}\,\mathrm{Im}\, g_2(t) & \ldots \\ 0 & 0 & 0 & 0 & \sqrt{2\kappa}\,\mathrm{Im}\, g_2(t) & \sqrt{2\kappa}\,\mathrm{Re}\, g_2(t) & \ldots \\ \vdots & \vdots & \vdots & \vdots & \vdots & \vdots & \ldots \end{pmatrix}. \tag{50}$$

Using Fourier transforms and the correlation function of the noises, one can derive the following general expression for the stationary output correlation matrix, which is the counterpart of the 4×4 intracavity relation of Eq. (15):

$$V^{\mathrm{out}} = \int d\omega \tilde{T}(\omega)\left(\tilde{M}^{\mathrm{ext}}(\omega) + \frac{P_{\mathrm{out}}}{2\kappa}\right) \times D^{\mathrm{ext}}(\omega)\left(\tilde{M}^{\mathrm{ext}}(\omega)^\dagger + \frac{P_{\mathrm{out}}}{2\kappa}\right)\tilde{T}(\omega)^\dagger, \tag{51}$$

where $P_{\mathrm{out}}=\mathrm{Diag}[0,0,1,1,\ldots]$ is the projector onto the $2N$-dimensional space associated with the output quadratures, and we have introduced the extensions corresponding to the matrices $\tilde{M}(\omega)$ and $D(\omega)$ of the previous section,

$$\tilde{M}^{\mathrm{ext}}(\omega) = (i\omega + A^{\mathrm{ext}})^{-1}, \tag{52}$$

with

$$A^{\mathrm{ext}}=\begin{pmatrix} 0 & \omega_m & 0 & 0 & 0 & 0 & \dots \\ -\omega_m & -\gamma_m & G & 0 & G & 0 & \dots \\ 0 & 0 & -\kappa & \Delta & 0 & 0 & \dots \\ G & 0 & -\Delta & -\kappa & 0 & 0 & \dots \\ 0 & 0 & 0 & 0 & -\kappa & \Delta & \dots \\ G & 0 & 0 & 0 & -\Delta & -\kappa & \dots \\ \vdots & \vdots & \vdots & \vdots & \vdots & \vdots & \dots \end{pmatrix} \quad (53)$$

and

$$D^{\mathrm{ext}}(\omega)=\begin{pmatrix} 0 & 0 & 0 & 0 & 0 & 0 & \dots \\ 0 & \frac{\gamma_m\omega}{\omega_m}\coth\left(\frac{\hbar\omega}{2k_BT}\right) & 0 & 0 & 0 & 0 & \dots \\ 0 & 0 & \kappa & 0 & \kappa & 0 & \dots \\ 0 & 0 & 0 & \kappa & 0 & \kappa & \dots \\ 0 & 0 & \kappa & 0 & \kappa & 0 & \dots \\ 0 & 0 & 0 & \kappa & 0 & \kappa & \dots \\ \vdots & \vdots & \vdots & \vdots & \vdots & \vdots & \dots \end{pmatrix}. \quad (54)$$

A deeper understanding of the general expression for V^{out} of Eq. (51) is obtained by multiplying the terms in the integral; one gets

$$V^{\mathrm{out}}=\int d\omega\, \tilde{T}(\omega)\tilde{M}^{\mathrm{ext}}(\omega)D^{\mathrm{ext}}(\omega)\tilde{M}^{\mathrm{ext}}(\omega)^{\dagger}\tilde{T}(\omega)^{\dagger}+\frac{P_{\mathrm{out}}}{2} + \frac{1}{2}\int d\omega\, \tilde{T}(\omega)[\tilde{M}^{\mathrm{ext}}(\omega)R_{\mathrm{out}}+R_{\mathrm{out}}\tilde{M}^{\mathrm{ext}}(\omega)^{\dagger}]\tilde{T}(\omega)^{\dagger}, \quad (55)$$

where $R_{\mathrm{out}}=P_{\mathrm{out}}D^{\mathrm{ext}}(\omega)/\kappa=D^{\mathrm{ext}}(\omega)P_{\mathrm{out}}/\kappa$ and we have used the fact that

$$\int \frac{d\omega}{4\kappa^2}\tilde{T}(\omega)P_{\mathrm{out}}D^{\mathrm{ext}}(\omega)P_{\mathrm{out}}\tilde{T}(\omega)^{\dagger}=\frac{P_{\mathrm{out}}}{2}. \quad (56)$$

The first integral term in Eq. (55) is the contribution coming from the interaction between the mechanical resonator and the intracavity field. The second term gives the noise added by the optical input noise to each output mode. The third term gives the contribution of the correlations between the intracavity mode and the optical input field, which may cancel the destructive effects of the second noise term and eventually even increase the optomechanical entanglement with respect to the intracavity case. We shall analyze this fact in the following section.

C. A single output mode

Let us first consider the case when we select and detect only one mode at the cavity output. Just to fix the ideas, we choose the mode specified by the filter function of Eqs. (42) and (44), with central frequency Ω and bandwidth τ^{-1}. Straightforward choices for this output mode are a mode centered either at the cavity frequency $\Omega=\omega_c-\omega_0$, or at the driving laser frequency $\Omega=0$ (we are in the rotating frame and

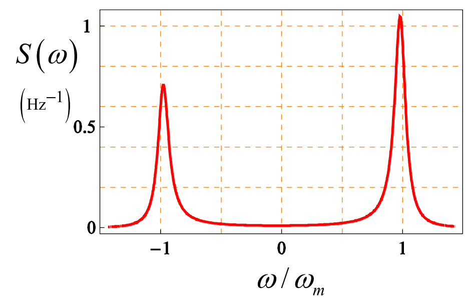

FIG. 4. (Color online) Cavity output spectrum in the case of an oscillator with $\omega_m/2\pi=10$ MHz, $\mathcal{Q}=10^5$, mass $m=50$ ng, a cavity of length $L=1$ mm with finesse $F=2\times10^4$, detuning $\Delta=\omega_m$, driven by a laser with input power $P=30$ mW and wavelength 810 nm, yielding $G_0=0.43$ kHz, $G=0.41\omega_m$, and a cavity bandwidth $\kappa=0.75\omega_m$. We have again assumed a reservoir temperature for the mirror of $T=0.4$ K, corresponding to $\bar{n}\simeq 833$. In this regime photons are scattered only at the two first motional sidebands, at $\omega_0\pm\omega_m$.

therefore all frequencies are referred to the laser frequency ω_0), and with a bandwidth of the order of the cavity bandwidth, $\tau^{-1}\simeq\kappa$. However, as discussed above, the motion of the mechanical resonator generates Stokes and anti-Stokes motional sidebands, consequently modifying the cavity output spectrum. Therefore it may be nontrivial to determine which is the optimal frequency bandwidth of the output field that carries most of the optomechanical entanglement generated within the cavity. The cavity output spectrum associated with the photon number fluctuations $S(\omega)=\langle\delta a(\omega)^{\dagger}\delta a(\omega)\rangle$ is shown in Fig. 4, where we have considered a parameter regime close to that considered for the intracavity case, i.e., an oscillator with $\omega_m/2\pi=10$ MHz, $\mathcal{Q}=10^5$, mass $m=50$ ng, a cavity of length $L=1$ mm with finesse $F=2\times10^4$, detuning $\Delta=\omega_m$, driven by a laser with input power $P=30$ mW and wavelength 810 nm, yielding $G_0=0.43$ kHz, $G=0.41\omega_m$, and a cavity bandwidth $\kappa=0.75\omega_m$. We have again assumed a reservoir temperature for the mirror of $T=0.4$ K, corresponding to $\bar{n}\simeq 833$. This regime is not far from but does not correspond to the best intracavity optomechanical entanglement regime discussed in Sec. III. In fact, optomechanical entanglement monotonically increases with the coupling G and is maximum just at the bistability threshold, which, however, is not a convenient operating point. We have chosen instead a smaller input power and a larger mass, implying a smaller value of G and an operating point not too close to threshold.

In order to determine the output optical mode that is best entangled with the mechanical resonator, we study the logarithmic negativity $E_{\mathcal{N}}$ associated with the output CM V^{out} of Eq. (55) (for $N=1$) as a function of the central frequency of the mode Ω and its bandwidth τ^{-1}, at the considered operating point. The results are shown in Fig. 5, where $E_{\mathcal{N}}$ is plotted versus Ω/ω_m at five different values of $\varepsilon=\tau\omega_m$. If $\varepsilon\lesssim 1$, i.e., the bandwidth of the detected mode is larger than ω_m, the detector does not resolve the motional sidebands, and $E_{\mathcal{N}}$ has a value (roughly equal to that of the intracavity case) which does not essentially depend upon the central frequency. For smaller bandwidths (larger ε), the sidebands are resolved by the detection, and the role of the central fre-

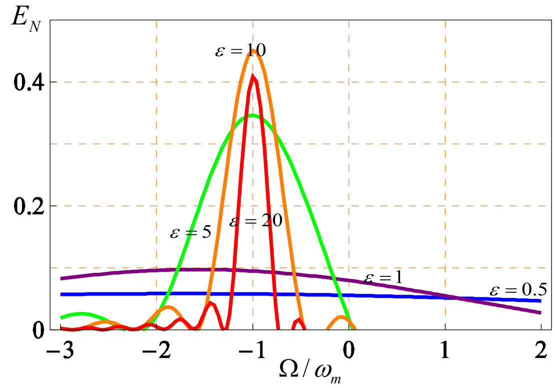

FIG. 5. (Color online) Logarithmic negativity $E_{\mathcal{N}}$ of the CV bipartite system formed by the mechanical mode and a single cavity output mode versus the central frequency of the detected output mode Ω/ω_m at five different values of its inverse bandwidth $\varepsilon=\omega_m\tau$. The other parameters are the same as in Fig. 4. When the bandwidth is not too large, the mechanical mode is significantly entangled only with the first Stokes sideband at $\omega_0-\omega_m$.

quency becomes important. In particular, $E_{\mathcal{N}}$ becomes highly peaked around the Stokes sideband $\Omega=-\omega_m$, showing that the optomechanical entanglement generated within the cavity is mostly carried by this lower-frequency sideband. What is relevant is that the optomechanical entanglement of the output mode is significantly larger than its intracavity counterpart and achieves its maximum value at the optimal value $\varepsilon\simeq 10$, i.e., a detection bandwidth $\tau^{-1}\simeq\omega_m/10$. This means that, in practice, by appropriately filtering the output light, one realizes an effective entanglement distillation because the selected output mode is more entangled than the intracavity mode with the mechanical resonator.

The fact that the output mode which is most entangled with the mechanical resonator is the one centered around the Stokes sideband is also consistent with the physics of two previous models analyzed in Refs. [55,75]. In [75] an atomic ensemble is inserted within the Fabry-Pérot cavity studied here, and one gets a system showing robust tripartite (atom-mirror-cavity) entanglement at the steady state only when the atoms are resonant with the Stokes sideband of the laser. In particular, the atomic ensemble and the mechanical resonator become entangled under this resonance condition, and this is possible only if entanglement is carried by the Stokes sideband because the two parties are only indirectly coupled through the cavity mode. In [55], a free-space optomechanical model is discussed, where the entanglement between a vibrational mode of a perfectly reflecting micromirror and the two first motional sidebands of an intense laser beam shone on the mirror is analyzed. In that case also the mechanical mode is entangled only with the Stokes mode and it is not entangled with the anti-Stokes sideband.

By looking at the output spectrum of Fig. 4, one can also understand why the output mode optimally entangled with the mechanical mode has a finite bandwidth $\tau^{-1}\simeq\omega_m/10$ (for the chosen operating point). In fact, the optimal situation is achieved when the detected output mode overlaps as much as possible with the Stokes peak in the spectrum, and therefore τ^{-1} coincides with the width of the Stokes peak. This width is

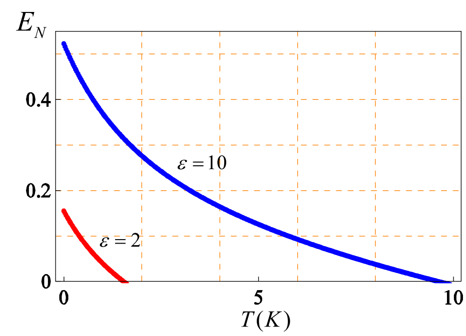

FIG. 6. (Color online) Logarithmic negativity $E_{\mathcal{N}}$ of the CV bipartite system formed by the mechanical mode and the cavity output mode centered around the Stokes sideband $\Omega=-\omega_m$ versus temperature for two different values of its inverse bandwidth $\varepsilon=\omega_m\tau$. The other parameters are the same as in Fig. 4.

determined by the effective damping rate of the mechanical resonator, $\gamma_m^{\mathrm{eff}}=\gamma_m+\Gamma$, given by the sum of the intrinsic damping rate γ_m and the net laser cooling rate Γ of Eq. (36). It is possible to check that, with the chosen parameter values, the condition $\varepsilon=10$ corresponds to $\tau^{-1}\simeq\gamma_m^{\mathrm{eff}}$.

It is finally important to analyze the robustness of the present optomechanical entanglement with respect to temperature. As discussed above and shown in [53], the entanglement of the resonator with the intracavity mode is very robust. It is important to see if this robustness is retained also by the optomechanical entanglement of the output mode. This is shown by Fig. 6, where the entanglement $E_{\mathcal{N}}$ of the output mode centered at the Stokes sideband $\Omega=-\omega_m$ is plotted versus the temperature of the reservoir at two different values of the bandwidth, the optimal one $\varepsilon=10$, and at a larger bandwidth $\varepsilon=2$. We see the expected decay of $E_{\mathcal{N}}$ for increasing temperature, but above all that also this output optomechanical entanglement is robust against temperature because it persists even above liquid He temperatures, at least in the case of the optimal detection bandwidth $\varepsilon=10$.

D. Two output modes

Let us now consider the case where we detect at the output two independent, well-resolved, optical output modes. We use again the steplike filter functions of Eqs. (42) and (44), assuming the same bandwidth τ^{-1} for both modes and two different central frequencies Ω_1 and Ω_2 satisfying the orthogonality condition of Eq. (43), $\Omega_1-\Omega_2=2p\pi\tau^{-1}$, for some integer p, in order to have two independent optical modes. It is interesting to analyze the stationary state of the resulting tripartite CV system formed by the two output modes and the mechanical mode, in order to see if and when it is able to show (i) purely optical bipartite entanglement between the two output modes; (ii) fully tripartite optomechanical entanglement.

The generation of two entangled light beams by means of the radiation-pressure interaction of these fields with a mechanical element has already been considered in various configurations. In Ref. [76], and more recently in Ref. [52], two modes of a Fabry-Pérot cavity system with a movable mirror, each driven by an intense laser, are entangled at the output

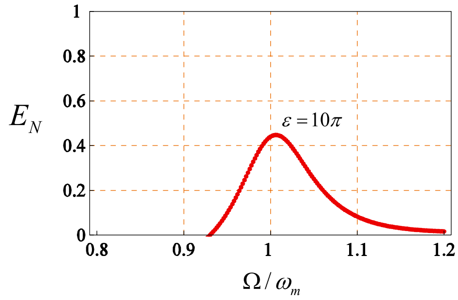

FIG. 7. (Color online) Logarithmic negativity $E_{\mathcal{N}}$ of the bipartite system formed by the output mode centered at the Stokes sideband ($\Omega_1=-\omega_m$) and a second output mode with the same inverse bandwidth ($\varepsilon=\omega_m\tau=10\pi$) and a variable central frequency Ω, plotted versus Ω/ω_m. The other parameters are the same as in Fig. 4. Optical entanglement is present only when the second output mode overlaps with the anti-Stokes sideband.

due to their common ponderomotive interaction with the movable mirror (the scheme was then generalized to many driven modes in [77]). In the single-mirror free-space model of Ref. [55], the two first motional sidebands are also robustly entangled by the radiation-pressure interaction as in a two-mode squeezed state produced by a nondegenerate parametric amplifier [78]. Robust two-mode squeezing of a bimodal cavity system can be similarly produced if the movable mirror is replaced by a single ion trapped within the cavity [79].

The situation considered here is significantly different from that of Refs. [52,76,77,79], which require many driven cavity modes, each associated with the corresponding output mode. In the present case instead, the different output modes *originate from the same single driven cavity mode*, and therefore it is much simpler from an experimental point of view. The present scheme can be considered as a sort of "cavity version" of the free-space case of Ref. [55], where the reflecting mirror is driven by a single intense laser. Therefore, as in [55,78], one expects to find a parameter region where the two output modes centered around the two motional sidebands of the laser are entangled. This expectation is clearly confirmed by Fig. 7, where the logarithmic negativity $E_{\mathcal{N}}$ associated with the bipartite system formed by the output mode centered at the Stokes sideband ($\Omega_1=-\omega_m$) and a second output mode with the same inverse bandwidth ($\varepsilon=\omega_m\tau=10\pi$) and a variable central frequency Ω, is plotted versus Ω/ω_m. $E_{\mathcal{N}}$ is calculated from the CM of Eq. (55) (for $N=2$), eliminating the first two rows associated with the mechanical mode, and assuming the same parameters considered in the former subsection for the single-output-mode case. One can clearly see that bipartite entanglement between the two cavity outputs exists only in a narrow frequency interval around the anti-Stokes sideband, $\Omega=\omega_m$, where $E_{\mathcal{N}}$ achieves its maximum. This shows that, as in [55,78], the two cavity output modes corresponding to the Stokes and anti-Stokes sidebands of the driving laser are significantly entangled by their common interaction with the mechanical resonator. The advantage of the present cavity scheme with respect to the free-space case of [55,78] is that the parameter regime for reaching radiation-pressure-mediated optical entanglement is much more promising from an experimental point of view because it requires less input power and a not too large mechanical quality factor of the resonator. In Fig. 8, the dependence of $E_{\mathcal{N}}$ of the two output modes centered at the two sidebands $\Omega=\pm\omega_m$ upon their inverse bandwidth ε is studied. We see that, differently from optomechanical entanglement of the previous subsection, the logarithmic negativity of the two sidebands always increases for decreasing bandwidth, and it achieves a significant value (~ 1), comparable to that achievable with parametric oscillators, for very narrow bandwidths. This fact can be understood from the fact that quantum correlations between the two sidebands are established by the coherent scattering of the cavity photons by the oscillator, and that the quantum coherence between the two scattering processes is maximal for output photons with frequencies $\omega_0\pm\omega_m$.

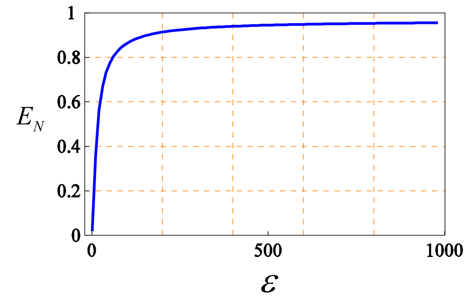

FIG. 8. (Color online) Logarithmic negativity $E_{\mathcal{N}}$ of the bipartite system formed by the two output modes centered at the Stokes and anti-Stokes sidebands ($\Omega=\pm\omega_m$) versus the inverse bandwidth $\varepsilon=\omega_m\tau$. The other parameters are the same as in Fig. 4.

In Fig. 9 we analyze the robustness of the entanglement between the Stokes and anti-Stokes sidebands with respect to the temperature of the mechanical resonator, by plotting, for the same parameter regime as in Fig. 8, $E_{\mathcal{N}}$ versus the temperature T at two different values of the inverse bandwidth ($\varepsilon=10\pi, 100\pi$). We see that this purely optical CV entanglement is extremely robust against temperature, especially in the limit of small detection bandwidth, showing that the effective coupling provided by radiation pressure can be strong enough to render optomechanical devices with high-quality resonators a possible alternative to parametric oscillators for

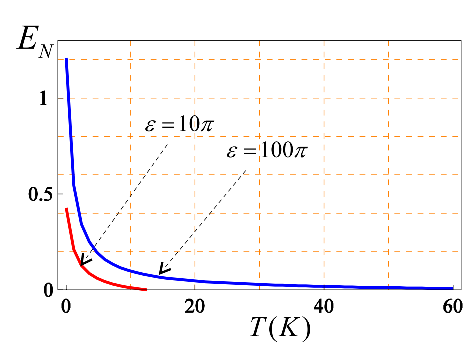

FIG. 9. (Color online) Logarithmic negativity $E_{\mathcal{N}}$ of the two output modes centered at the Stokes and anti-Stokes sidebands ($\Omega=\pm\omega_m$) versus the temperature of the resonator reservoir, at two different values of the inverse bandwidth $\varepsilon=\omega_m\tau$. The other parameters are the same as in Fig. 4.

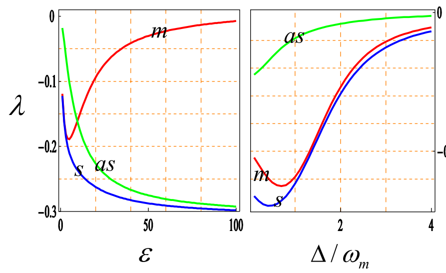

FIG. 10. (Color online) Analysis of tripartite entanglement. The minimum eigenvalues after partial transposition with respect to the Stokes mode (blue line), anti-Stokes mode (green line), and mechanical mode (red line) are plotted versus the inverse bandwidth ε at $\Delta=\omega_m$ in the left plot, and versus the cavity detuning Δ/ω_m at fixed inverse bandwidth $\varepsilon=\pi$ in the right plot. The other parameters are the same as in Fig. 4. These eigenvalues are all negative in the studied intervals, showing that one has fully tripartite entanglement.

the generation of entangled light beams for CV quantum communication.

Since in Figs. 7 and 8 we used the same parameter values for the cavity-resonator system used in Fig. 5, we have that, in this parameter regime, the output mode centered around the Stokes sideband mode shows bipartite entanglement simultaneously with the mechanical mode and with the anti-Stokes sideband mode. This fact suggests that, in this parameter region, the CV tripartite system formed by the output Stokes and anti-Stokes sidebands and the mechanical resonator mode could be characterized by a fully tripartite-entangled stationary state. This is confirmed by Fig. 10, where we have applied the classification criterion of Ref. [80], providing a necessary and sufficient criterion for the determination of the entanglement class in the case of tripartite CV Gaussian states, which is directly computable in terms of the eigenvalues of appropriate test matrices [80]. These eigenvalues are plotted in Fig. 10 versus the inverse bandwidth ε at $\Delta=\omega_m$ in the left plot, and versus the cavity detuning Δ/ω_m at a fixed inverse bandwidth $\varepsilon=\pi$ in the right plot (the other parameters are again those of Fig. 4). We see that all the eigenvalues are negative in a wide interval of detuning and detection bandwidth of the output modes, showing, as expected, that we have a fully tripartite-entangled steady state.

Therefore, if we consider the system formed by the two cavity output fields centered around the two motional sidebands at $\omega_0 \pm \omega_m$ and the mechanical resonator, we find that the entanglement properties of its steady state are identical to those of the analogous tripartite optomechanical free-space system of Ref. [55]. In fact, the Stokes output mode shows bipartite entanglement both with the mechanical mode and with the anti-Stokes mode; the anti-Stokes mode is not entangled with the mechanical mode, but the whole system is in a fully tripartite-entangled state for a wide parameter regime. What is important is that in the present cavity scheme such a parameter regime is much easier to achieve with respect to that of the free-space case.

V. CONCLUSIONS

We have studied in detail the entanglement properties of the steady state of a driven optical cavity coupled by radiation pressure to a micromechanical oscillator, extending in various directions the results of Ref. [53]. We first analyzed the intracavity steady state and showed that the cavity mode and the mechanical element can be entangled in a robust way against temperature. We have also investigated the relationship between entanglement and cooling of the resonator by the back action of the cavity mode, which has already been demonstrated recently in Refs. [11,12,14,15,18–20] and discussed theoretically in Refs. [23,28–31]. We have seen that a significant back action cooling is a sufficient but not necessary condition for achieving entanglement. In fact, intracavity entanglement is possible also in the opposite regime of negative detunings Δ, where the cavity mode *drives* and does not cool the resonator, even though it is not robust against temperature in this latter case. Moreover, entanglement is not optimal when cooling is optimal, because the logarithmic negativity is maximized close to the stability threshold of the system, where instead cooling is not achieved.

We then extended our analysis to the cavity output, which is more important from a practical point of view because any quantum-communication application involves the manipulation of traveling optical fields. We have developed a general theory showing how it is possible to define and evaluate the entanglement properties of the multipartite system formed by the mechanical resonator and N independent output modes of the cavity field.

We then applied this theory and saw that, in the parameter regime corresponding to a significant intracavity entanglement, the tripartite system formed by the mechanical element and the two output modes centered at the first Stokes and anti-Stokes sidebands of the driving laser (where the cavity output noise spectrum is concentrated) shows robust fully tripartite entanglement. In particular, the Stokes output mode is strongly entangled with the mechanical mode and shows a sort of entanglement distillation because its logarithmic negativity is significantly larger than the intracavity one when its bandwidth is appropriately chosen.

In the same parameter regime, the Stokes and anti-Stokes sideband modes are robustly entangled, and the achievable entanglement in the limit of a very narrow detection bandwidth is comparable to that generated by a parametric oscillator. These results make the present cavity optomechanical system very promising for the realization of CV quantum-information interfaces and networks.

ACKNOWLEDGMENTS

This work has been supported by the European Commission (programs QAP), and by INFN (SQUALO project).

[1] M. P. Blencowe, Phys. Rep. **395**, 159 (2004).
[2] K. C. Schwab and M. L. Roukes, Phys. Today **58** (7), 36 (2005).
[3] T. J. Kippenberg and K. J. Vahala, Opt. Express **15**, 17172 (2007).
[4] V. B. Braginsky and F. Ya Khalili, *Quantum Measurements* (Cambridge University Press, Cambridge, U.K., 1992).
[5] W. Marshall, C. Simon, R. Penrose, and D. Bouwmeester, Phys. Rev. Lett. **91**, 130401 (2003).
[6] P. F. Cohadon, A. Heidmann, and M. Pinard, Phys. Rev. Lett. **83**, 3174 (1999).
[7] M. D. LaHaye, O. Buu, B. Camarota, and K. C. Schwab, Science **304**, 74 (2004).
[8] C. H. Metzger and K. Karrai, Nature (London) **432**, 1002 (2004).
[9] A. Naik, O. Buu, M. D. LaHaye, A. D. Armour, A. A. Clerk, M. P. Blencowe, and K. C. Schwab, Nature (London) **443**, 193 (2006).
[10] O. Arcizet, P.-F. Cohadon, T. Briant, M. Pinard, A. Heidmann, J. M. Mackowski, C. Michel, L. Pinard, O. Francais, and L. Rousseau, Phys. Rev. Lett. **97**, 133601 (2006).
[11] S. Gigan, H. Böhm, M. Paternostro, F. Blaser, G. Langer, J. Hertzberg, K. Schwab, D. Bäuerle, M. Aspelmeyer, and A. Zeilinger, Nature (London) **444**, 67 (2006).
[12] O. Arcizet, P.-F. Cohadon, T. Briant, M. Pinard, and A. Heidmann, Nature (London) **444**, 71 (2006).
[13] D. Kleckner and D. Bouwmeester, Nature (London) **444**, 75 (2006).
[14] A. Schliesser, P. Del'Haye, N. Nooshi, K. J. Vahala, and T. J. Kippenberg, Phys. Rev. Lett. **97**, 243905 (2006).
[15] T. Corbitt, Y. Chen, E. Innerhofer, H. Müller-Ebhardt, D. Ottaway, H. Rehbein, D. Sigg, S. Whitcomb, C. Wipf, and N. Mavalvala, Phys. Rev. Lett. **98**, 150802 (2007); T. Corbitt, C. Wipf, T. Bodiya, D. Ottaway, D. Sigg, N. Smith, S. Whitcomb, and N. Mavalvala, *ibid.* **99**, 160801 (2007).
[16] M. Poggio, C. L. Degen, H. J. Mamin, and D. Rugar, Phys. Rev. Lett. **99**, 017201 (2007).
[17] K. R. Brown, J. Britton, R. J. Epstein, J. Chiaverini, D. Leibfried, and D. J. Wineland, Phys. Rev. Lett. **99**, 137205 (2007).
[18] S. Groblacher, S. Gigan, H. R. Boehm, A. Zeilinger, and M. Aspelmeyer, Europhys. Lett. **81**, 54003 (2008).
[19] A. Schliesser, R. Rivière, G. Anetsberger, O. Arcizet, and T. J. Kippenberg, Nat. Phys. **4**, 415 (2008).
[20] J. D. Thompson, B. M. Zwickl, A. M. Jayich, F. Marquardt, S. M. Girvin, and J. G. E. Harris, Nature (London) **452**, 72 (2008).
[21] C. A. Regal, J. D. Teufel, and K. W. Lehnert, Nat. Phys. **4**, 555 (2008).
[22] S. Mancini, D. Vitali, and P. Tombesi, Phys. Rev. Lett. **80**, 688 (1998).
[23] V. B. Braginsky, S. E. Strigin, and S. P. Vyatchanin, Phys. Lett. A **287**, 331 (2001).
[24] J.-M. Courty, A. Heidmann, and M. Pinard, Eur. Phys. J. D **17**, 399 (2001).
[25] D. Vitali, S. Mancini, L. Ribichini, and P. Tombesi, Phys. Rev. A **65**, 063803 (2002); **69**, 029901(E) (2004); J. Opt. Soc. Am. B **20**, 1054 (2003).
[26] I. Wilson-Rae, P. Zoller, and A. Imamoglu, Phys. Rev. Lett. **92**, 075507 (2004).
[27] I. Martin, A. Shnirman, L. Tian, and P. Zoller, Phys. Rev. B **69**, 125339 (2004).
[28] F. Marquardt, J. P. Chen, A. A. Clerk, and S. M. Girvin, Phys. Rev. Lett. **99**, 093902 (2007).
[29] I. Wilson-Rae, N. Nooshi, W. Zwerger, and T. J. Kippenberg, Phys. Rev. Lett. **99**, 093901 (2007).
[30] C. Genes, D. Vitali, P. Tombesi, S. Gigan, and M. Aspelmeyer, Phys. Rev. A **77**, 033804 (2008).
[31] A. Dantan, C. Genes, D. Vitali, and M. Pinard, Phys. Rev. A **77**, 011804(R) (2008).
[32] M. P. Blencowe and M. N. Wybourne, Physica B **280**, 555 (2000).
[33] P. Rabl, A. Shnirman, and P. Zoller, Phys. Rev. B **70**, 205304 (2004); X. Zhou and A. Mizel, Phys. Rev. Lett. **97**, 267201 (2006); K. Jacobs, *ibid.* **99**, 117203 (2007); W. Y. Huo and G. L. Long, Appl. Phys. Lett. **92**, 133102 (2008).
[34] R. Ruskov, K. Schwab, and A. N. Korotkov, Phys. Rev. B **71**, 235407 (2005); A. A. Clerk, F. Marquardt, and K. Jacobs, e-print arXiv:0802.1842v1; M. J. Woolley, A. C. Doherty, G. J. Milburn, and K. C. Schwab, e-print arXiv:0803.1757v1 [quant-ph].
[35] J. S. Bell, Physics (Long Island City, N.Y.) **1**, 195 (1964).
[36] B. Julsgaard *et al.*, Nature (London) **413**, 400 (2001).
[37] A. J. Berkley *et al.*, Science **300**, 1548 (2003).
[38] S. Mancini, V. Giovannetti, D. Vitali, and P. Tombesi, Phys. Rev. Lett. **88**, 120401 (2002).
[39] A. D. Armour, M. P. Blencowe, and K. C. Schwab, Phys. Rev. Lett. **88**, 148301 (2002).
[40] J. Eisert, M. B. Plenio, S. Bose, and J. Hartley, Phys. Rev. Lett. **93**, 190402 (2004).
[41] X. Zou and W. Mathis, Phys. Lett. A **324**, 484 (2004).
[42] A. N. Cleland and M. R. Geller, Phys. Rev. Lett. **93**, 070501 (2004).
[43] L. Tian and P. Zoller, Phys. Rev. Lett. **93**, 266403 (2004).
[44] L. Tian, Phys. Rev. B **72**, 195411 (2005).
[45] F. Xue, Y. X. Liu, C. P. Sun, and F. Nori, Phys. Rev. B **76**, 064305 (2007).
[46] A. K. Ringsmuth and G. J. Milburn, J. Mod. Opt. **54**, 2223 (2007).
[47] D. Vitali, P. Tombesi, M. J. Woolley, A. C. Doherty, and G. J. Milburn, Phys. Rev. A **76**, 042336 (2007).
[48] J. Zhang, K. Peng, and S. L. Braunstein, Phys. Rev. A **68**, 013808 (2003).
[49] M. Pinard, A. Dantan, D. Vitali, O. Arcizet, T. Briant, and A. Heidmann, Europhys. Lett. **72**, 747 (2005).
[50] M. Paternostro, D. Vitali, S. Gigan, M. S. Kim, C. Brukner, J. Eisert, and M. Aspelmeyer, Phys. Rev. Lett. **99**, 250401 (2007).
[51] M. Bhattacharya and P. Meystre, Phys. Rev. Lett. **99**, 073601 (2007); **99**, 153603 (2007); M. Bhattacharya, H. Uys, and P. Meystre, Phys. Rev. A **77**, 033819 (2008).
[52] C. Wipf, T. Corbitt, Y. Chen, and N. Mavalvala, e-print arXiv:0803.4001v1 [quant-ph].
[53] D. Vitali, S. Gigan, A. Ferreira, H. R. Böhm, P. Tombesi, A. Guerreiro, V. Vedral, A. Zeilinger, and M. Aspelmeyer, Phys. Rev. Lett. **98**, 030405 (2007).
[54] D. Vitali, S. Mancini, and P. Tombesi, J. Phys. A: Math. Theor. **40**, 8055 (2007).
[55] S. Mancini, D. Vitali, and P. Tombesi, Phys. Rev. Lett. **90**, 137901 (2003); S. Pirandola, S. Mancini, D. Vitali, and P. Tombesi, Phys. Rev. A **68**, 062317 (2003).

[56] S. Pirandola, S. Mancini, D. Vitali, and P. Tombesi, J. Mod. Opt. **51**, 901 (2004).
[57] S. Pirandola, D. Vitali, P. Tombesi, and S. Lloyd, Phys. Rev. Lett. **97**, 150403 (2006).
[58] T. J. Kippenberg, H. Rokhsari, T. Carmon, A. Scherer, and K. J. Vahala, Phys. Rev. Lett. **95**, 033901 (2005).
[59] C. Genes, D. Vitali, and P. Tombesi, e-print arXiv:0803.2788v1 [quant-ph].
[60] V. Giovannetti and D. Vitali, Phys. Rev. A **63**, 023812 (2001).
[61] M. Pinard, Y. Hadjar, and A. Heidmann, Eur. Phys. J. D **7**, 107 (1999).
[62] C. K. Law, Phys. Rev. A **51**, 2537 (1995).
[63] C. W. Gardiner and P. Zoller, *Quantum Noise* (Springer, Berlin, 2000).
[64] L. Landau and E. Lifshitz, *Statistical Physics* (Pergamon, New York, 1958).
[65] L. Diósi, Phys. Rev. A **78**, 021801(R) (2008).
[66] T.-C. Zhang, J. P. Poizat, P. Grelu, J.-F Roch, P. Grangier, F. Marin, A. Bramati, V. Jost, M. D. Levenson, and E. Giacobino, Quantum Semiclassic. Opt. **7**, 601 (1995).
[67] S. Mancini and P. Tombesi, Phys. Rev. A **49**, 4055 (1994).
[68] I. S. Gradshteyn and I. M. Ryzhik, *Table of Integrals, Series and Products* (Academic Press, Orlando, FL, 1980), p. 1119.
[69] R. Benguria and M. Kac, Phys. Rev. Lett. **46**, 1 (1981).
[70] J. Eisert, Ph.D. thesis, University of Potsdam, 2001; G. Vidal and R. F. Werner, Phys. Rev. A **65**, 032314 (2002); G. Adesso, A. Serafini, and F. Illuminati, *ibid.* **70**, 022318 (2004).
[71] R. Simon, Phys. Rev. Lett. **84**, 2726 (2000).
[72] C. W. Gardiner and P. Zoller, *Quantum Noise* (Ref. [63]), p. 71.
[73] M. S. Kim, W. Son, V. Bužek, and P. L. Knight, Phys. Rev. A **65**, 032323 (2002).
[74] S. J. van Enk and C. A. Fuchs, Phys. Rev. Lett. **88**, 027902 (2001); D. Vitali, P. Canizares, J. Eschner, and G. Morigi, New J. Phys. **10**, 033025 (2008).
[75] C. Genes, D. Vitali, and P. Tombesi, Phys. Rev. A **77**, 050307(R) (2008).
[76] V. Giovannetti, S. Mancini, and P. Tombesi, Europhys. Lett. **54**, 559 (2001).
[77] S. Giannini, S. Mancini, and P. Tombesi, Quantum Inf. Comput. **3**, 265–279 (2003).
[78] S. Pirandola, S. Mancini, D. Vitali, and P. Tombesi, J. Opt. B: Quantum Semiclassical Opt. **5**, S523 (2003).
[79] G. Morigi, J. Eschner, S. Mancini, and D. Vitali, Phys. Rev. Lett. **96**, 023601 (2006); Phys. Rev. A **73**, 033822 (2006); D. Vitali, G. Morigi, and J. Eschner, *ibid.* **74**, 053814 (2006).
[80] G. Giedke, B. Kraus, M. Lewenstein, and J. I. Cirac, Phys. Rev. A **64**, 052303 (2001).